Formation and Transformation of Five Different Phases in the $CaSO_4-H_2O$ System: Crystal Structure of the Subhydrate β-$CaSO_4 \cdot 0.5H_2O$ and Soluble Anhydrite $CaSO_4$

Axel Nørlund Christensen,[†] Maja Olesen,[‡] Yngve Cerenius,[§] and Torben R. Jensen*[,‡]

Crystal Chemistry, Højkolvej 7, DK-8210 Århus V, Denmark, Interdisciplinary Nanoscience Centre (iNANO), Department of Chemistry, University of Aarhus, DK-8000 Århus C, Denmark, and MAX-laboratory, Lund University, S-22100 Lund, Sweden

Received September 26, 2007. Revised Manuscript Received January 3, 2008

At least five crystalline phases can be found in the $CaSO_4-H_2O$ system, which are gypsum $CaSO_4 \cdot 2H_2O$, the subhydrates α- and β-$CaSO_4 \cdot 0.5H_2O$, and the soluble and insoluble anhydrite $CaSO_4$. The formation of these five phases in the $CaSO_4-H_2O$ system and their transformations were investigated by *in situ* time-resolved synchrotron radiation powder X-ray diffraction (SR-PXD) in this study. Furthermore, revised structural models for β-$CaSO_4 \cdot 0.5H_2O$ and soluble anhydrite $CaSO_4$ are presented. The hydration of α-$CaSO_4 \cdot 0.5H_2O$ was studied at 25 °C and showed that the reaction with H_2O started immediately after mixing the two reactants and that the formation of $CaSO_4 \cdot 2H_2O$ was coupled to the depletion of α-$CaSO_4 \cdot 0.5H_2O$. The thermal decomposition of $CaSO_4 \cdot 2H_2O$ was investigated in the temperature range of 25−500 °C and showed the formation of α-$CaSO_4 \cdot 0.5H_2O$ followed by the formation of soluble anhydrite AIII-$CaSO_4$, which was gradually converted to insoluble anhydrite AII-$CaSO_4$. The thermal decomposition of α-$CaSO_4 \cdot 0.5D_2O$ was investigated in the temperature range of 25−500 °C and showed successive phase transformations to β-$CaSO_4 \cdot 0.5D_2O$, soluble anhydrite AIII-$CaSO_4$, and insoluble anhydrite AII-$CaSO_4$. The two polymorphs of anhydrite coexist in the investigated temperature range of 200−500 °C. The hydrothermal decomposition of $CaSO_4 \cdot 2H_2O$ was investigated in the temperature range of 25−200 °C using a 1 M HNO_3 or a 1 M LiCl solution, and in both experiments, $CaSO_4 \cdot 2H_2O$ was converted to α-$CaSO_4 \cdot 0.5H_2O$ and further to insoluble anhydrite AII-$CaSO_4$. A structural model for β-$CaSO_4 \cdot 0.5H_2O$ is proposed on the basis of SR-PXD data and a trigonal unit cell (in hexagonal setting) $a = 6.931\ 45(3)$, $c = 12.736\ 17(4)$ Å, $Z = 6$, and space group $P3_1$. A structural model for soluble anhydrite AIII-$CaSO_4$ is also proposed on the basis of powder neutron diffraction data, and a hexagonal unit cell parameters are $a = 6.9687(1)$, $c = 6.3004(1)$ Å, $Z = 3$, and space group $P6_222$.

1. Introduction

Gypsum $CaSO_4 \cdot 2H_2O$ is a central material in the modern world as an important constituent in construction materials, e.g., as an additive for the production of cements or the production of gypsum wallboards.[1,2] Calcium sulfates are also used in biocompatible materials, e.g., as bone void filler.[3,4] Calcium sulfates are produced in large quantities in the process of removing sulfur oxides from the exhaust gas from coal-driven power plants.[5–7] At least five crystalline phases are described in the literature to be found in the $CaSO_4-H_2O$ system: gypsum $CaSO_4 \cdot 2H_2O$, the subhydrates α-$CaSO_4 \cdot 0.5H_2O$ and β-$CaSO_4 \cdot 0.5H_2O$, and the soluble and insoluble anhydrites of $CaSO_4$, denoted AIII and AII, respectively, and several of those are described with more than one structural model. A detailed knowledge of their stability and the physical and chemical conditions for their transformations is crucial for applications of $CaSO_4$-based materials; e.g., in the industrial production of "Plaster of Paris", efforts are made to obtain a product with a minimum amount of insoluble anhydrite (AII-$CaSO_4$).[8]

Several calcium sulfate materials, $CaSO_4 \cdot xH_2O$, where $0 \leq x \leq 2$, are known from the literature, both synthetic and found in nature as minerals. Table 1 lists structural data for some of those materials and reveals some discrepancy. Gypsum occurs commonly in nature as tabular transparent or slightly colored crystals called selenite, as a fine grained variety called alabaster, as desert rose, which is gypsum with brown sand inclusions, and as gypsum rock, where the gypsum contains impurities of anhydrite, calcite, dolomite, and clays.[9] Anhydrite is a rare mineral because it transforms

* To whom correspondence should be addressed: Interdisciplinary Nanoscience Center (iNANO), Department of Chemistry, University of Aarhus, Langelandsgade 140, DK-8000 Aarhus C, Denmark. Telephone: +45-8942-3894. Fax: +45-8619-6199. E-mail: trj@chem.au.dk.
[†] Crystal Chemistry.
[‡] University of Aarhus.
[§] Lund University.

(1) Harder, J. *ZKG Int.* **2005**, *58*, 18.
(2) Solberg, C.; Evju, C.; Emanuelson, A.; Hansen, S. *ZKG Int.* **2002**, *55*, 94.
(3) Doadrio, J. C.; Arcos, D.; Cabanas, M. V.; Vallet-Regi, M. *Biomaterials* **2004**, *25*, 2629.
(4) Pietrzak, W. S.; Ronk, R. *J. Craniofacial Surg.* **2000**, *11*, 327.
(5) Fernandez, J.; Renedo, M. J.; Pesquera, A.; Irabien, J. A. *Powder Technol.* **2001**, 119–201.
(6) Lee, K.; Teong, B.; Subhash, M.; Abdul, R. *Energy Sources* **2006**, *28*, 1241.
(7) Dathe, H.; Jentys, A.; Haider, P.; Schreier, E.; Fricke, R.; Lercher, J. A. *Phys. Chem. Chem. Phys.* **2006**, *8*, 1601.
(8) Vagt, O. *Can. Miner. Yearbook* **1994**, 25.125.8.
(9) Gypsum mineral in http://webmineral.com/data/Gypsum.shtml.

10.1021/cm7027542 CCC: $40.75
Published on Web 02/26/2008

Table 1. Crystallographic Data for Compounds Found in the $CaSO_4-H_2O$ System

name and formula	unit cell parameters						space group	reference
			Gypsum					
$CaSO_4 \cdot 2H_2O$	5.679	15.202	6.522	90	118.43	90	*I*2/a	10
	5.679	15.202	6.522	90	118.43	90	*I*2/a	11
	6.286	15.213	5.678	90	114.1	90	*C*2/c	12
			Calcium Sulfate Subhydrates					
α-$CaSO_4 \cdot 0.5H_2O$	11.94	6.83	12.70	90	90.60	90	*C*121	13
α-$CaSO_4 \cdot 0.67H_2O$	12.028	6.927	12.67	90	90.21	90	*I*2	14
α-$CaSO_4 \cdot 0.53H_2O$	12.028	6.931	12.692	90	90.18	90	*I*2	15
α-$CaSO_4 \cdot 0.5H_2O$	12.034	6.929	12.676	90	90.265	90	*I*121	16
β-$CaSO_4 \cdot 0.5H_2O$	6.9372	6.9372	6.345	90	90	120	*P*3121	17
β-$CaSO_4 \cdot 0.8H_2O$	6.968	6.968	6.410	90	90	120	*P*3121	18
β-$CaSO_4 \cdot 0.62H_2O$	13.861	13.861	12.739	90	90	120		15
β-$CaSO_4 \cdot 0.6H_2O$	11.989	6.930	12.753	90	90.0	90	*I*121	16
			Anhydrite					
$CaSO_4$ (soluble)	6.982	6.982	6.340	90	90	120	$P6_222$	19
	6.969	6.969	6.303	90	90	120	$P6_222$	20
	12.078	6.972	6.304	90	90	90	*C*222	16
			Anhydrite					
$CaSO_4$ (insoluble)	7.006	6.998	6.245	90	90	90	*A*mma	21

to the more common mineral gypsum by a reaction with water. The calcium sulfate subhydrates α- and β-$CaSO_4 \cdot 0.5H_2O$ have distinct powder diffraction patterns and therefore different structures and possibly also different water contents and values in the range of 0.5−0.8, which are listed in Table 1, found by crystal structure analysis. α-$CaSO_4 \cdot 0.5H_2O$ is formed by dehydration in an acidic aqueous suspension of $CaSO_4 \cdot 2H_2O$ or at hydrothermal conditions in the presence of electrolytes, whereas β-$CaSO_4 \cdot 0.5H_2O$ is formed by dehydration of $CaSO_4 \cdot 2H_2O$ in a water vapor atmosphere at temperatures over 100 °C.[22] The crystal structures and phase transformations of these phases have been studied for decades but remain not fully understood. Bezou et al. determined the compositions of the two subhydrates as α-$CaSO_4 \cdot 0.5H_2O$ and β-$CaSO_4 \cdot 0.6H_2O$ and confirmed a monoclinic structure for the α-$CaSO_4 \cdot 0.5H_2O$ and suggested a monoclinic structure for β-$CaSO_4 \cdot 0.6H_2O$.[23] The monoclinic space group *C*121 with a unit cell volume of 529.8 Å^3 was suggested for the structure of β-$CaSO_4 \cdot 0.6H_2O$.[24] However, the β-$CaSO_4 \cdot 0.6H_2O$ structure was subsequently described in the monoclinic space group *I*121 with the unit cell volume 1058.8 Å^3 and with $\beta = 90°$.[16]

This structural discrepancy has prompted the present investigation using *in situ* mixing of the reactants on the diffractometer and following the reactions by *in situ* time-resolved synchrotron radiation powder X-ray diffraction (SR-PXD). The advent of powerful synchrotron X-ray radiation facilities has allowed for the development of a number of experimental techniques for material sciences. The short exposure time of the individual diffractogram and high-resolution detectors have provided new insight into material sciences at the atomic level. Advanced design of sample holders allow for studies of solid/liquid or solid/gas systems and changes in physical and chemical conditions during data acquisition, such as pressure, temperature, or *in situ* mixing of chemicals.[25–28] The latter is important for the study of relatively fast chemical reactions.[29–31] Examples of such studies are *in situ* investigation of catalytic activity,[32] crystallization of zeolite A,[33] the kinetics of formation of porous metal-substituted AlPO phases,[34] transformation of iron-containing oxides and hydroxides,[35,36] studies of early hydration reactions of cements,[29] chemical reactions in the setting of Sorel's cement,[37] and the study of hydration of cement and clinker phases.[30] Some of the above-mentioned techniques are used in the present study of structures and transformations of phases found in the $CaSO_4-H_2O$ system.

This work is performed with focus on the phase transitions between gypsum $CaSO_4 \cdot 2H_2O$, the subhydrates α- and β-$CaSO_4 \cdot 0.5H_2O$, and the anhydrites of $CaSO_4$, studying the reactions under hydrothermal or dry conditions. In the following paper, the two subhydrates will be mentioned with the composition $CaSO_4 \cdot 0.5H_2O$, if the water content is undetermined from experimental data.

(10) Pedersen, B. F.; Semmingsen, D. *Acta Crystallogr., Sect. B: Struct. Sci.* **1982**, *38*, 1074.
(11) Schofield, P. F.; Knight, K. S.; Stretton, I. C. *Am. Mineral.* **1996**, *81*, 847.
(12) de la Torre, Á. G.; López-Olmo, M.-G.; Álvarez-Rua, C.; Garcia-Granda, S.; Aranda, M. A. G. *Powder Diffr.* **2004**, *19*, 240.
(13) Gallitelli, P. *Period. Mineral.* **1933**, *4*, 1.
(14) Bushuev, N. N.; Borisov, V. M.; Russ, J. *Inorg. Chem.* **1982**, *37*, 341.
(15) Kuzel, H. J.; Hauner, M. *Zem. Kalk Gips, B* **1987**, *40*, 628.
(16) Bezou, C.; Nonat, A.; Mutin, J.-C.; Christensen, A. N.; Lehmann, M. S. *J. Solid State Chem.* **1995**, *117*, 165.
(17) Abriel, W.; Nesper, R. *Z. Kristallogr.* **1993**, *205*, 99.
(18) Abriel, W. *Acta Crystallogr., Sect. C: Cryst. Struct. Commun.* **1983**, *39*, 956.
(19) Flörke, O. W. *Neues Jahrb. Mineral., Monatsh.* **1952**, *84*, 189.
(20) Lager, G. A.; Armbruster, T.; Rotella, F. J.; Jorgensen, J. D.; Hinks, D. G. *Am. Mineral.* **1984**, *69*, 910.
(21) Kirfel, A.; Will, G. *Acta Crystallogr., Sect. B: Struct. Sci.* **1980**, *36*, 2881.
(22) Folner, S.; Wolter, A.; Preusser, A.; Indris, S.; Silber, C.; Folner, H. *Cryst. Res. Technol.* **2002**, *37*, 1075.
(23) Bezou, C.; Mutin, J.-C.; Nonat, A. *J. Chim. Phys.* **1990**, *87*, 1257.
(24) Bezou, C.; Christensen, A. N.; Cox, D.; Lehmann, M. S.; Nonat, A. *C. R. Acad. Sci. Paris* **1991**, *312*, 43.
(25) Jensen, T. R.; Christensen, A. N.; Hanson, J. C. *Cem. Concr. Res.* **2005**, *35*, 2300.
(26) Bösenberg, U.; Doppiu, S.; Mosegaard, L.; Barkhordarian, G.; Eigen, N.; Borgschulte, A.; Jensen, T. R.; Cerenius, Y.; Gutfleisch, O.; Klassen, T.; Dornheim, M.; Bormann, R. *Acta Mater.* **2007**, *55*, 3951.
(27) Barkhordarian, G.; Jensen, T. R.; Doppiu, S.; Bösenberg, U.; Borgschulte, A.; Gremau, R.; Cerenius, Y.; Dornheim, M.; Klassen, T.; Bormann, R. *J. Phys. Chem. C* **2008**, *112*, 2743–2749.

Table 2. Experimental Details for the Performed *in Situ* SR-PXD Experiments[a]

number	reactants	T_{max} (°C)	sample holder	λ (Å)
1	α-$CaSO_4 \cdot 0.5H_2O$[b]	25	SiO_2	1.0010
2	$CaSO_4 \cdot 2H_2O$[c]	450	Al_2O_3	1.1250
3	$CaSO_4 \cdot 2H_2O$[b]	200	SiO_2	1.0010
4	α-$CaSO_4 \cdot 0.5D_2O$[c]	500	Al_2O_3	1.0010
5	$CaSO_4 \cdot 2H_2O$[d]	190	Al_2O_3	1.1072
6	$CaSO_4 \cdot 2H_2O$[e]	190	Al_2O_3	1.1072

[a] All experiments are performed with the heating rate of 5.0 °C/min in the temperature range from room temperature to T_{max} using either a sapphire single crystal tube (Al_2O_3) or a quartz glass (SiO_2) capillary as the sample container. [b] Aqueous suspension. [c] Heating of a dry solid. [d] Suspension in an aqueous solution of 1 M LiCl. [e] Suspension in an aqueous solution of 1 M HNO_3.

2. Experimental Section

The *in situ* time-resolved SR-PXD experiments were performed at beam line I711 at the synchrotron radiation facility MAX II at MAX-laboratory in Lund, Sweden, using a MAR165 CCD detector.[38] The selected X-ray wavelengths were 1.0010, 1.1072, or 1.1250 Å, and the X-ray exposure time was 30 or 60 s. A number of experiments were conducted using a specially constructed sample cell for studies of solid/gas and solid/liquid reactions in the temperature range from room temperature to 500 °C.[39] A sapphire single-crystal tube (Al_2O_3, 0.79 mm i.d.) or a quartz glass capillary (SiO_2, 0.7 mm o.d.) was used as a sample holder. A gas supply system allows for a nitrogen gas pressure to be applied, which prevents the solutions from boiling. A filament is heating the sample during X-ray data acquisition, and the temperature is measured with a thermocouple. SR-PXD raw data were converted to powder diffraction profiles using FIT2D.[40] The full width at half-maximum for some selected reflections of synchrotron powder patterns are listed below to indicate the resolution of these powder patterns.

Three different materials were used in six *in situ* SR-PXD experiments (see Table 2). The materials were gypsum $CaSO_4 \cdot 2H_2O$ and calcium sulfate hemihydrate, α-$CaSO_4 \cdot 0.5H_2O$ from J. T. Baker (analyzed), used as received. A deuterated sample of calcium sulfate subhydrate, α-$CaSO_4 \cdot 0.5D_2O$, was prepared using 99.7% D_2O as described previously for a similar sample using H_2O.[16] The purity of the materials were investigated by powder X-ray diffraction (PXD) measured at 25 °C on a Stoe Stadi powder diffractometer using Cu $K\alpha_1$ radiation, $\lambda = 1.5406$ Å. A position-sensitive linear detector was used in a step scan mode. The patterns of the samples were in agreement with ICDD card number 83-438 for α-$CaSO_4 \cdot 0.5H_2O$ (bassanite) and ICDD card number 21-816 for $CaSO_4 \cdot 2H_2O$ (selenite); however, the dihydrate sample from J. T. Baker contained an impurity of α-$CaSO_4 \cdot 0.5H_2O$. A Rietveld quantitative phase analysis using pattern number 5 at 33 °C (experiment number 2), the reported structure of $CaSO_4 \cdot 2H_2O$[11] and α-$CaSO_4 \cdot 0.5H_2O$,[16] and FullProf gave a α-$CaSO_4 \cdot 0.5H_2O$ content of 19.8% of the sample.[41]

Hydration of α-$CaSO_4 \cdot 0.5H_2O$ in Neutral Solution (Experiment Number 1). A quartz glass capillary (0.7 mm o.d.) placed in a vertical position was loaded with α-$CaSO_4 \cdot 0.5H_2O$, and the sample was slightly compacted to approximately 2 mm. Water was introduced in the capillary with a syringe, so that the meniscus was ca. 2 mm from the dry sample. The water contained less than 0.01% of a detergent, which reduces the surface tension of water and improves the wetting of the dry sample. The capillary was mounted horizontally at the diffractometer and connected via a nylon tube to a gas supply system. After a few diffraction patterns at 25 °C of the dry sample were measured, the pressure of the capillary was raised to $p(N_2) = 13$ bar. This brings water in contact with the dry sample, *in situ* during data acquisition, and the hydration reaction starts.

Thermal Decomposition (Experiment Numbers 2 and 4). The dry powder of $CaSO_4 \cdot 2H_2O$ or α-$CaSO_4 \cdot 0.5D_2O$ was placed in the sample holder and fixed with quartz glass wool. This prevents the powder form moving during decomposition.

Hydrothermal Decomposition Experiments (Experiment Numbers 3, 5, and 6). The samples were prepared by grinding ca. 0.1 g of the solid material, $CaSO_4 \cdot 2H_2O$, with ca. 0.5 mL of either water or aqueous solutions of either 1.0 M HNO_3 or 1.0 M LiCl in a mortar. The suspensions were injected into a sapphire tube using a syringe. The sample was pressurized with nitrogen gas to $p(N_2) = 13$ bar and heated from 25 °C to a maximum temperature of 190 °C using a heating rate of 5.0 °C/min.

Reinvestigation of the Structure of β-$CaSO_4 \cdot 0.5H_2O$. The two materials α- and β-$CaSO_4 \cdot 0.5H_2O$ show powder diffraction patterns with some overlapping reflections but also clear differences mainly among the weak reflections. Originally, a monoclinic structural model was selected to describe the structure of β-$CaSO_4 \cdot 0.5H_2O$, space group $I121$, $a = 11.989$, $b = 6.930$, $c = 12.753$ Å, $\beta = 90.0°$, $V = 1059.6$ Å^3.[16] This choice was made so that both unit cell and packing of atoms in the model for β-$CaSO_4 \cdot 0.5H_2O$ resembled that of the model for α-$CaSO_4 \cdot 0.5H_2O$. However, the monoclinic β-$CaSO_4 \cdot 0.5H_2O$ structure has $\beta = 90.0°$, which is unusual, and for this reason, the structure of β-$CaSO_4 \cdot 0.5H_2O$ was reinvestigated in this study.[42]

A selected powder pattern (number 25) of β-$CaSO_4 \cdot 0.5D_2O$, obtained in the *in situ* experiment number 4 (at $T = 160$ °C, see below) could be indexed on a trigonal/hexagonal unit cell with $a = 6.9434(2)$, $c = 12.5759(6)$ Å, and $V = 525.1$ Å^3 using DICVOL04.[44] To test this choice of unit cell, the high-resolution SR-PXD data from ref 16 was used with the same procedure. To include a few very weak reflections, two of the unit cell axes need to be doubled, giving a super cell, $a = 13.8637(4)$, $c = 12.7360(7)$ Å, and $V = 2119.9$ Å^3. A unit cell of this size has been observed previously.[15] Profile fitting using FullProf gave the following for the two cells: $a = 13.8630(1)$, $c = 12.7362(1)$ Å, $R_{Bragg} = 0.173$, $R_F = 1.438$ and $a = 6.9315(1)$, $c = 12.7363(1)$ Å, $R_{Bragg} = 0.061$, $R_F = 0.237$, respectively.[41] It was decided to use the smaller cell with the low R_F value to find a structural model for β-$CaSO_4 \cdot 0.5H_2O$, which also gives a more reasonable data/parameter ratio.

The pattern combined with the direct method program EXPO and the space group $P3_1$ gave a solution with two Ca and two S atom positions.[45] The z coordinate of one Ca atom was adjusted, $z = 0.0$, to fix the origin of the model. This model was then used in

(28) Mosegaard, L.; Møller, B.; Jøorgensen, J.-E.; Hanson, J. C.; Cerenius, Y.; Besenbacher, F.; Jensen, T. R. *J. Alloys Compd.* **2007**, *446–447*, 301–305.
(29) Barnes, P.; Clark, S. M.; Häusermann, D.; Henderson, E.; Fentiman, C. H.; Muhamad, M. N.; Rashid, S. *Phase Transitions* **1992**, *39*, 117.
(30) Christensen, A. N.; Scarlett, N. V. Y.; Madsen, I. C.; Jensen, T. R.; Hanson, J. C. *J. Chem. Soc., Dalton Trans.* **2003**, 1529.
(31) Barnes, P.; Turrillas, X.; Jupe, A. C.; Colston, S. L.; O'Connor, D.; Cernik, R. J.; Livesey, P.; Hall, C.; Bates, D.; Dennis, R. *J. Chem. Soc., Faraday Trans.* **1996**, *92*, 2187.
(32) Clausen, B. S.; Steffensen, G.; Fabius, B.; Villadsen, J.; Feidenfans'l, R.; Topsø, H. *J. Catal.* **1991**, *132*, 524.
(33) Norby, P.; Christensen, A. N.; Hanson, J. C. In *Zeolites and Related Microporous Materials: State of the Art, 1999. Studies in Surface Science and Catalysis*; Weitkamp, J., Karge, H. G., Pfeifer, H., Hölderich, W., Eds.; Elsevier, Amsterdam, The Netherlands, 1994; Vol. 84, p 179.
(34) Christensen, A. N.; Jensen, T. R.; Norby, P.; Hanson, J. C. *Chem. Mater.* **1998**, *10*, 1688.
(35) Christensen, A. N.; Jensen, T. R.; Bahl, C. R. H.; DiMasi, E. *J. Solid State Chem.* **2007**, *180*, 1431.
(36) Jørgensen, J.-E.; Mosegaard, L.; Thomsen, L. E.; Jensen, T. R.; Hanson, J. C. *J. Solid State Chem.* **2007**, *180*, 179.

Table 3. Refined Parameters for the Structure of β-$CaSO_4 \cdot 0.5H_2O$ Using the Space Group $P3_1$[a]

atom	*x/a*	*y/b*	*z/c*	*B* (Å^2)
Ca1	0.662(5)	0.881(4)	0.0	2.0
Ca2	0.119(3)	0.781(3)	0.832(4)	2.0
S1	0.654(4)	0.878(4)	0.251(3)	2.0
O11	0.536(9)	0.996(7)	0.304(5)	2.0
O12	0.586(9)	0.665(9)	0.193(4)	2.0
O13	0.833(9)	1.057(9)	0.180(5)	2.0
O14	0.785(9)	0.848(8)	0.331(4)	2.0
S2	0.123(5)	0.778(5)	0.077(2)	2.0
O21	−0.051(9)	0.793(7)	0.011(5)	2.0
O22	0.020(9)	0.570(9)	0.154(4)	2.0
O23	0.335(9)	0.912(13)	0.009(4)	2.0
O24	0.157(10)	0.931(8)	0.168(5)	2.0
OW	0.570(10)	0.327(11)	0.151(4)	2.0

[a] The unit cell parameters were a = 6.931 45(3) Å and c = 12.736 17(4) Å. Refinement parameters: zero point = 0.0083(6)°, U = 0.047(3), V = −0.024(6), W = 0.005(3), X = 0.010(2), and Y = 0.022(2). R_{Bragg} = 9.40%, and R_F = 10.67%. The previously reported structure using the same set of data only has R values for the profile-matching mode calculations. Calculated interatomic distances: the S−O bonds within the sulfate ions are from 1.45 to 1.57 Å. Ca1−O = 2.19−2.81 Å and Ca2−O = 2.26−2.99 Å. The coordination numbers for Ca1 and Ca2 are 8 and 9, respectively. Ca2 includes coordination to a water molecule. The data were measured at 25 °C.

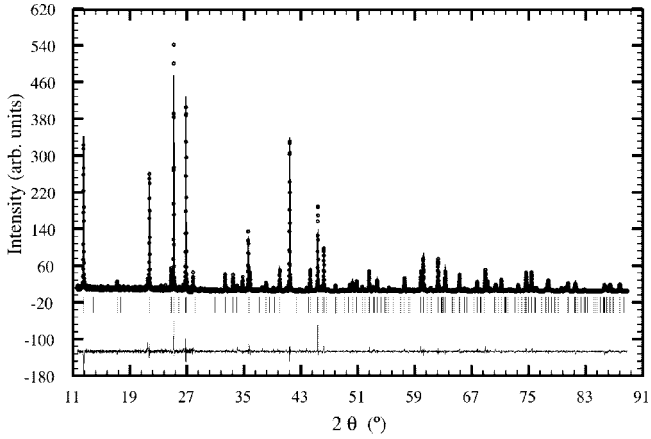

Figure 1. Rietveld refinement of the crystal structure of β-$CaSO_4 \cdot 0.5H_2O$ using high-resolution SR-PXD data from ref 16 shown as observed (symbols) and calculated (line) patterns and a difference plot (R_{Bragg} = 9.40%, R_F = 10.67%, and λ = 1.3075 Å).

the *ab initio* structure solving program FOX,[46] where two Ca and two S atom positions were fixed and where two SO_4 tetrahedra were introduced as rigid bodies (S−O distances of 1.49 Å) and allowed to turn around the fixed S atom positions. This gave a model, which was used in a second FOX calculation, where one H_2O molecule was introduced as a rigid body molecule and allowed to move; the atoms from the previous calculation were kept fixed. The final model was used in a Rietveld refinement of the structure using FullProf.[41,47] The results of the refinements are listed in Table 3. Figure 1 displays the observed, calculated, and difference diffraction patterns.

Reinvestigation of the Structure of Soluble Anhydrite, AIII-$CaSO_4$. The structure of soluble anhydrite AIII-$CaSO_4$ is expected to be similar to the structure of β-$CaSO_4 \cdot 0.5H_2O$; therefore, the previously suggested orthorhombic structure was reinvestigated in this study. The pattern from experiment number 4, pattern number 40 (T = 242 °C), and the high-resolution powder neutron diffraction pattern were indexed with the indexing program DICVOL04.[16,44] Two solutions were found, a hexagonal cell with a = 6.9799(4), c = 6.3117(7) Å, and V = 266.6 Å^3 and an orthorhombic cell with a = 6.311(1), b = 6.045(1), c = 3.489(1) Å, and V = 133.1 Å^3.[44] The hexagonal cell, which resembles the previously reported cell was used for profile matching.[20] For the neutron diffraction pattern, this gave the refined unit cell parameters a = 6.9686(1) and c = 6.3005(1) Å, using the space group $P6_222$ and the wavelength 1.5930 Å. A Rietveld refinement was performed using the reported structural model as start parameters.[20,47] The results are listed in Table 4. Figure 2 displays the observed, calculated, and difference patterns.

Table 4. Refined Parameters for the Structure of Soluble Anhydrite, AIII-$CaSO_4$, Using Space Group $P6_222$[a]

atom	*x/a*	*y/b*	*z/c*	*B* (Å^2)
Ca	0.5	0.0	0.0	0.66(4)
S	0.5	0.0	0.5	0.46(6)
O	0.4471(2)	0.1365(2)	0.3591(2)	0.98(2)

[a] The unit cell parameters were a = 6.968 65(3) and c = 6.300 44(4) Å. Refinement parameters: zero point = 0.0565(6)°, U = 0.080(3), V = −0.191(6), W = 0.171(3), X = 0.0, and Y = 0.085(2). Asymmetry parameters: $A1$ = −0.292(2), $A2$ = −0.173(1), $A3$ = 0.895(4), and $A4$ = 0.440(2). The first reflection is asymmetric, and the fit is not perfect. R_{Bragg} = 5.0%, R_F = 2.6%, and R_{wp} = 13.0%. The previously reported values for the structure using the same set of data and 11 positional parameters were R_{Bragg} = 7.6%, R_F = 4.8%, and R_{wp}= 10.9%. Calculated interatomic distances: Ca−O = 2.551(1) Å, Ca−O = 2.376(1) Å, and S−O = 1.477(1) Å. The coordination number for the Ca atom is 8. The data were measured at 25 °C.

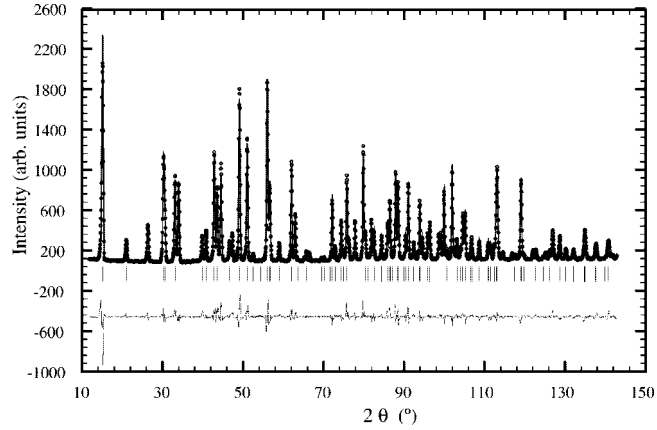

Figure 2. Rietveld refinement of the crystal structure of AIII-$CaSO_4$ using powder neutron diffraction data[16] and FullProf illustrated as observed (symbols) and calculated (line) patterns and a difference plot (R_{Bragg} = 5.0%, R_F = 2.6%, and λ = 1.5930 Å). The first reflection is asymmetric, and the fit is not perfect.

3. Results and Discussions

Structural Relation between the Phases Observed in the $CaSO_4-H_2O$ System. Bezou et al. determined the experimental conditions for the synthesis of α- and β-$CaSO_4 \cdot 0.5H_2O$, as pure phases.[23] The two forms have different chemical behavior, e.g., their reactions with water,[22] and also physical properties, such as NMR-spectroscopic parameters and X-ray powder diffraction patterns. Therefore, α- and β-$CaSO_4 \cdot 0.5H_2O$ are expected to have similar but distinct crystal structures. Different unit cell volumes have

(37) Christensen, A. N.; Norby, P.; Hanson, J. C. *Acta Chem. Scand.* **1995**, *49*, 331.
(38) Cerenius, Y.; Ståhl, K.; Svensson, L. A.; Ursby, T.; Oskarsson, Å.; Albertsson, J.; Lijas, A. *J. Synchrotron Radiat.* **2000**, *7*, 203.
(39) Rodriguez, J. A.; Hanson, J. C.; Frenkel, A. I.; Kim, J. Y.; Perez, M. *J. Am. Chem. Soc.* **2002**, *124*, 346.

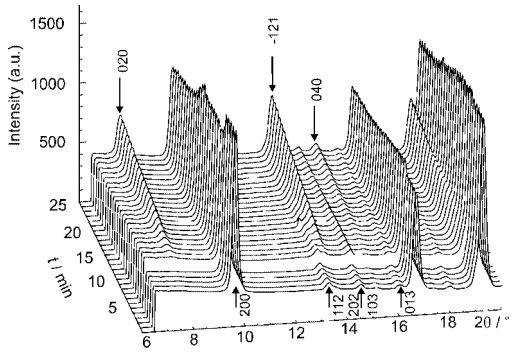

Figure 3. Stack of SR-PXD patterns measured at room temperature showing the hydration of α-$CaSO_4 \cdot 0.5H_2O$ (experiment number 1). Water was introduced into the dry powder (*in situ*) after pattern number 5. Miller indices for α-$CaSO_4 \cdot 0.5H_2O$ are below the curves, and Miller indices for $CaSO_4 \cdot 2H_2O$ are above the curves (λ = 1.0010 Å). Selected Bragg reflections in pattern number 28 have full width at half-maximum of $\Delta 2\theta$ = 0.294° and 0.235° for $CaSO_4 \cdot 2H_2O$ (020) and α-$CaSO_4 \cdot 0.5H_2O$ (200), respectively.

been suggested for the trigonal β-subhydrate, 264.4,[17] 269.5,[18] and 2119.6 $Å^3$,[15] and the volume 1059.6 $Å^3$ for the monoclinic cell used to describe the structure.[16] A number of investigations have not taken the existence of the two crystalline subhydrates into account nor have specified which of the two crystalline forms were used in the reported investigations.[48–50]

Soluble anhydrite and the two subhydrates have a channel structure. Soluble anhydrite is in this investigation described in the space group $P6_222$, where the structure has only 3 positional parameters for the atoms, compared to 11 positional parameters for the atoms in the space group $C222$.[16] The structure of soluble anhydrite in the setting ($P6_222$) is similar to the previously reported model.[20] The structure of β-$CaSO_4 \cdot 0.5H_2O$ is described in the space group $P3_1$ based on synchrotron X-ray powder diffraction data. The structure has columns of alternating Ca and SO_4 stacked in the c direction of the structure. It is planned to determine the water content and hydrogen bonding from powder neutron diffraction data of β-$CaSO_4 \cdot 0.5H_2O$.

Hydration of the Calcium Sulfate Subhydrate α-$CaSO_4 \cdot 0.5H_2O$ (Experiment Number 1). Figure 3 displays a stack of SR-PXD patterns for the hydration of α-$CaSO_4 \cdot 0.5H_2O$. Water was injected *in situ* into the dry powder using an elevated pressure of nitrogen during X-ray data acquisition, visible as an increase in the background level between pattern numbers 5 and 6. The hydration reaction starts immediately, observed by Bragg reflections from $CaSO_4 \cdot 2H_2O$ and as a decrease in the diffracted intensity from α-$CaSO_4 \cdot 0.5H_2O$. The depletion of α-$CaSO_4 \cdot 0.5H_2O$ is coupled with the increase in quantity of $CaSO_4 \cdot 2H_2O$. This observation contradicts a previous investigation by powder neutron diffraction and *ex situ* mixing of α-$CaSO_4 \cdot 0.5D_2O$ and D_2O,[51] which suggested that a large quantity of $CaSO_4 \cdot 0.5D_2O$ was converted to an amorphous phase prior to the formation of $CaSO_4 \cdot 2D_2O$. The crystallization of $CaSO_4 \cdot 2H_2O$ is observed to start immediately at room temperature even without the addition of nuclei of the compound, in contrast to a previous investigation.[48] The powder diffraction rings of α-$CaSO_4 \cdot 0.5H_2O$ had spots indicating relatively large crystallite grains in contrast to more coherent rings from $CaSO_4 \cdot 2H_2O$. This indicates a fast nucleation of gypsum that produces a large number of rather small crystallites of $CaSO_4 \cdot 2H_2O$, nucleating and growing from a dissolution of α-$CaSO_4 \cdot 0.5H_2O$. No intermediate or amorphous phase was observed in this study, in contrast to a previous powder neutron diffraction study, where an amorphous phase was suggested to be present.[51]

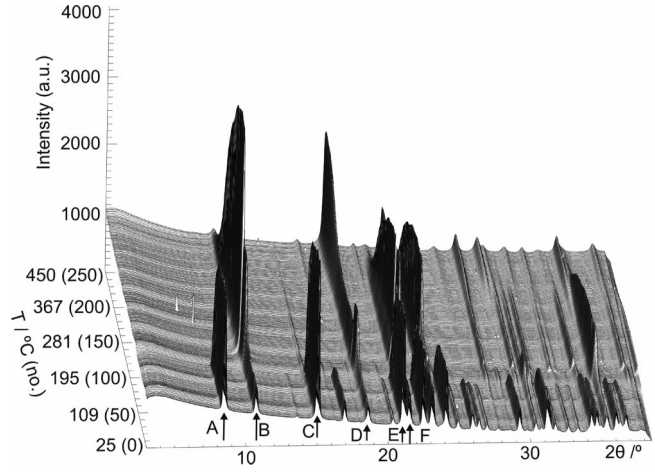

Figure 4. Stack of SR-PXD patterns showing the thermal decomposition of $CaSO_4 \cdot 2H_2O$ with an impurity of α-$CaSO_4 \cdot 0.5H_2O$ in the temperature range from 25 to 462 °C. The reflections marked with A, C, and E are from $CaSO_4 \cdot 2H_2O$, and the reflections marked with B, D, and F are from α-$CaSO_4 \cdot 0.5H_2O$ (λ = 1.1250 Å).

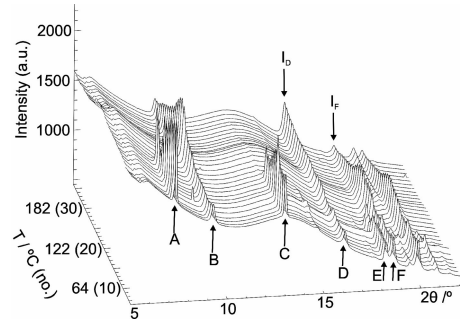

Figure 5. Stack of SR-PXD patterns showing the hydrothermal decomposition of $CaSO_4 \cdot 2H_2O$ (with an impurity of α-$CaSO_4 \cdot 0.5H_2O$) and the formation of β-$CaSO_4 \cdot 0.5H_2O$ and, subsequently, soluble anhydrite, AIII-$CaSO_4$, in the temperature range of 58−200 °C (experiment number 3). The reflections A, C, and E are from $CaSO_4 \cdot 2H_2O$, and the reflections B, D, and F are from α-$CaSO_4 \cdot 0.5H_2O$ (λ = 1.1010 Å). The Bragg reflections in pattern number 5 have full width at half-maximum of $\Delta 2\theta$ = 0.091° for the (020) $CaSO_4 \cdot 2H_2O$ reflection A and 0.181° for the (200) α-$CaSO_4 \cdot 0.5H_2O$ and, in pattern number 21, $\Delta 2\theta$ = 0.196° for the (200) β-$CaSO_4 \cdot 0.5H_2O$ reflection B.

(40) Hammersley, A. P.; Svensson, S. O.; Hanfland, M.; Fitch, A. N.; Hausermann, D. *High Pressure Res.* **1996**, *14*, 235.
(41) Rodríguez-Carvajal, J. *Physica B* **1993**, *192*, 55.
(42) The published atomic coordinates[16] for the crystal structure of β-$CaSO_4 \cdot 0.5H_2O$ (space group $I121$) can describe the packing of atoms in a trigonal/hexagonal cell, which is close to fulfill the symmetry of the space group $P3_1$ or the space group $P3_121$.[22] This hypothesis for the model of the structure was tested in the previous investigation[16] but was rejected, possibly because at that time EDINP[43] had a bug in the calculation of the trigonal/hexagonal symmetry.
(43) Pawley, G. S. *J. Appl. Crystallogr.* **1980**, *13*, 630.
(44) Boultif, A.; Louër, D. *J. Appl. Crystallogr.* **2004**, *37*, 724.
(45) Altomare, A.; Burla, M. C.; Camalli, M.; Carrozzini, B.; Cascarano, G. L.; Giacovazzo, C.; Guagliardi, A.; Moliterni, A. G. G.; Polidori, G.; Rizzi, R. *J. Appl. Crystallogr.* **1999**, *32*, 339.

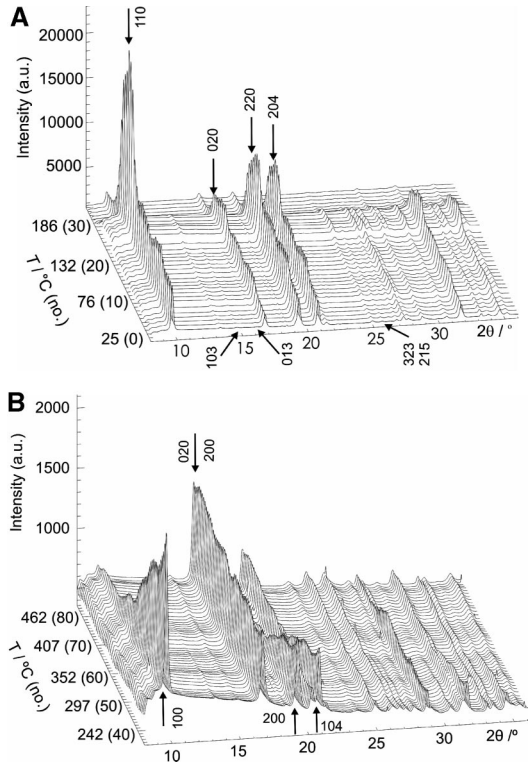

Figure 6. (A) Stack of powder patterns showing the thermal transformation of α- to β-$CaSO_4 \cdot 0.5D_2O$ followed by decomposition to soluble anhydrite, AIII-$CaSO_4$ (experiment number 4). Miller indices for some of the weak reflections of α-$CaSO_4 \cdot 0.5D_2O$ are below the curves, and Miller indices for some reflections of β-$CaSO_4 \cdot 0.5D_2O$ are indicated above the curves (λ = 1.0010 Å). (B) Stack of powder patterns showing the thermal transformation of soluble anhydrite, AIII-$CaSO_4$, to insoluble anhydrite, AII-$CaSO_4$ (experiment number 4). Miller indices for some reflections of soluble anhydrite (ICDD card number 43-606) are below the curves, and Miller indices for insoluble anhydrite (ICDD card number 37-1496) are above the curves (λ = 1.0010 Å).

Thermal Decomposition of $CaSO_4 \cdot 2H_2O$ (Experiment Number 2). Figure 4 displays a stack of SR-PXD patterns for the thermal decomposition of $CaSO_4 \cdot 2H_2O$ containing ca. 20% α-$CaSO_4 \cdot 0.5H_2O$ in the temperature range of 25−462 °C. The strong reflections marked with A, C, and E are from $CaSO_4 \cdot 2H_2O$ and B, D, and F are from α-$CaSO_4 \cdot 0.5H_2O$. The patterns up to number 50 at 109 °C show reflections of the original sample. A phase change is observed in the temperature range of 109−140 °C (patterns from numbers 50−68), where $CaSO_4 \cdot 2H_2O$ is converted to α-$CaSO_4 \cdot 0.5H_2O$. The α phase is observed up to the pattern number 83 and show decreasing diffracted intensity in the temperature range of 165−172 °C (numbers 83−87), where it is converted to soluble anhydrite, AIII-$CaSO_4$. The pattern of α-$CaSO_4 \cdot 0.5H_2O$, at 162 °C (number 80), corresponds to the unit cell parameters a = 12.092(3) Å, b = 6.976(1) Å, c = 12.755(1) Å, and β = 90.28(1)°, and the pattern of AIII-$CaSO_4$ measured at 196 °C (number 100) has the unit cell parameters a = 7.0144(4) and c = 6.3586(6) Å. Soluble anhydrite is slowly converted to insoluble anhydrite, AII-$CaSO_4$, in the temperature range of 280−462 °C (numbers 150−255). The PXD pattern of AII-$CaSO_4$ at 461 °C (number 255) corresponds to the unit cell parameters a = 7.0211(9) Å, b = 7.0347(11) Å, and c = 6.3242(6) Å, determined by a profile-matching calculation. The AIII- to AII-$CaSO_4$ phase transition occur in a relatively wide temperature range and is dependent upon the experimental conditions, such as the heating rate (see below, experiment number 4).

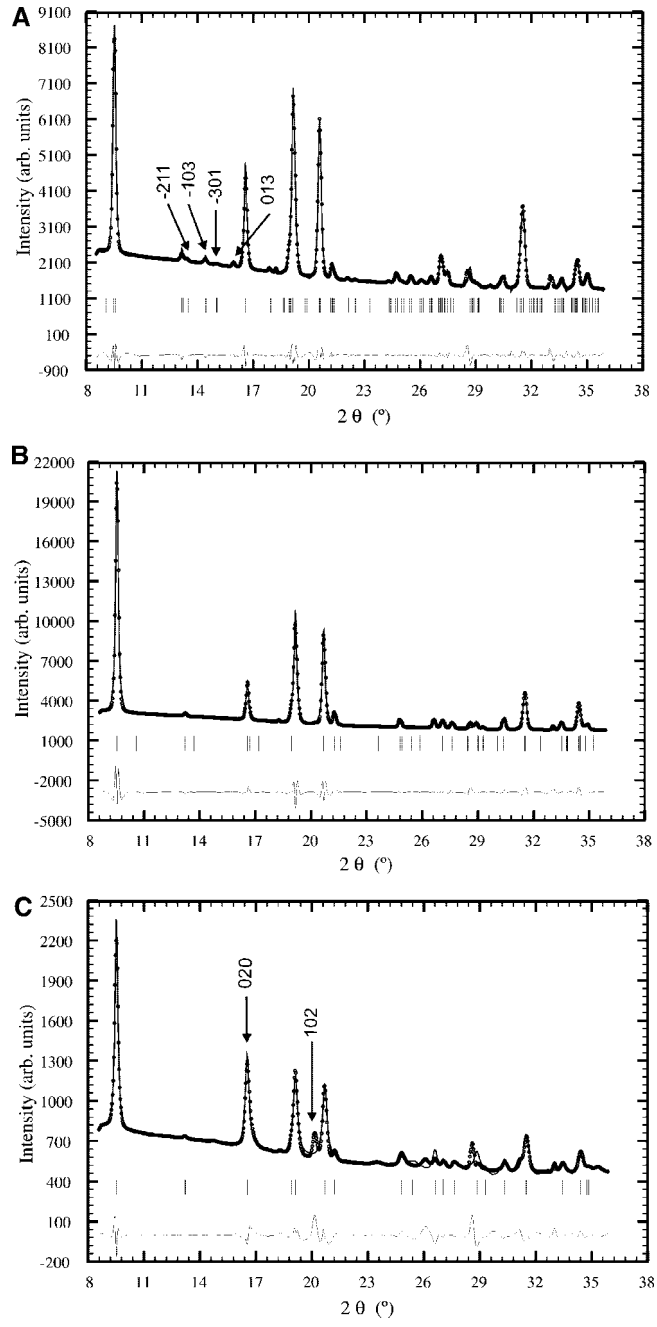

Figure 7. (A) Powder pattern of α-$CaSO_4 \cdot 0.5D_2O$ measured at 104 °C (PXD number 15 in experiment number 4). The profile-matching Rietveld refinement yields the intensity I = 1131 of the first strong reflection at 2θ = 9.628° and the background level I_{bgr} = 2298 at 2θ = 11.0°. The full width at the half-maximum of this 200 reflection is $\Delta 2\theta$ = 0.196°. (B) SR-PXD pattern of β-$CaSO_4 \cdot 0.5D_2O$ measured at 160 °C (PXD number 25 in experiment number 4). The profile-matching Rietveld refinement yields the intensity I = 3266 of the first strong reflection at 2θ = 9.584° and the background level I_{bgr} = 3047 at 2θ = 11.0°. The full width at the half-maximum of this 110 reflection is $\Delta 2\theta$ = 0.197°. (C) SR-PXD pattern of soluble anhydrite, AIII-$CaSO_4$, measured at 222 °C (PXD number 36). The profile-matching Rietveld refinement yields the intensity I = 444 of the first strong 100 reflection at 2θ = 9.578° ($\Delta 2\theta$ = 0.225°) and the background level I_{bgr} = 757 at 2θ = 11.0°. The pattern has reflections from insoluble anhydrite, AII-$CaSO_4$, marked with arrows.

Hydrothermal Decomposition of $CaSO_4 \cdot 2H_2O$ (Experiment Number 3). Figure 5displays a stack of powder patterns for the hydrothermal decomposition of $CaSO_4 \cdot 2H_2O$

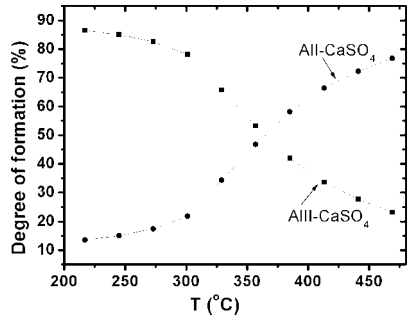

Figure 8. Degree of decomposition and formation of soluble anhydrite, AIII-$CaSO_4$, and insoluble anhydrite, AII-$CaSO_4$, versus the temperature in the temperature interval from approximately 200 to 500 °C.

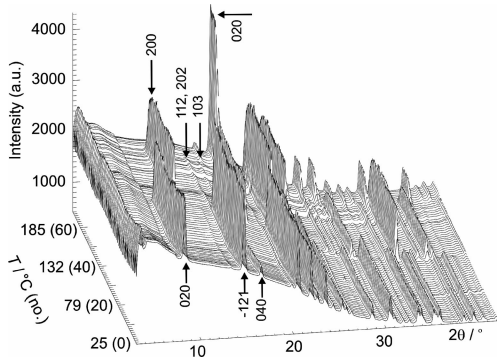

Figure 9. Stack of SR-PXD patterns showing the hydrothermal transformation of $CaSO_4 \cdot 2H_2O$ in a 1 M HNO_3 solution to α-$CaSO_4 \cdot 0.5H_2O$ at 118 °C and to insoluble anhydrite AII-$CaSO_4$ at 190 °C (experiment number 6). Miller indices for selected reflections of $CaSO_4 \cdot 2H_2O$ are below the curves, and Miller indices for α-$CaSO_4 \cdot 0.5H_2O$ are above the curves. Insoluble anhydrite AII-$CaSO_4$ is indicated by a horizontal arrow. The full width at half-maximum for the (020) $CaSO_4 \cdot 2H_2O$ reflection in pattern number 1 is $\Delta 2\theta = 0.255°$, $\Delta 2\theta = 0.250°$ for the (200) α-$CaSO_4 \cdot 0.5H_2O$ reflection in pattern number 50, and $\Delta 2\theta = 0.270°$ for the combined (200) plus (020) reflection of insoluble anhydrite, AII-$CaSO_4$, in pattern number 68.

in the temperature range of 59−200 °C (numbers 6−36). In this hydrothermal treatment, $CaSO_4 \cdot 2H_2O$ is converted to α-$CaSO_4 \cdot 0.5H_2O$ at 99 °C and α-$CaSO_4 \cdot 0.5H_2O$ is converted to β-$CaSO_4 \cdot 0.5H_2O$ at 118 °C. The β phase is observed in the temperature range of 118−163 °C (pattern numbers 19−27). It can be observed that the background level in this temperature range is slightly elevated, which is best seen at $2\theta = 5°$. β-$CaSO_4 \cdot 0.5H_2O$ is converted to AIII-$CaSO_4$ at 169 °C (number 28). The reflections marked with B, D, and F in Figure 5 are thus overlapping reflections from the three phases α-$CaSO_4 \cdot 0.5H_2O$, β-$CaSO_4 \cdot 0.5H_2O$, and AIII-$CaSO_4$, although with slightly different values of their *d* spacings. This makes it difficult to distinguish the three phases using observed *d* spacings. However, the intensities for the B, D, and F reflections are markedly different; e.g., for β-$CaSO_4 \cdot 0.5H_2O$ at 152 °C (pattern number 25), the ratio I_D/I_F is approximately 0.6, whereas for AIII-$CaSO_4$, the ratio $I_D/I_F \approx 2.8$ at 200 °C (number 36). To distinguish the three phases from each other, it is necessary to focus on the weak reflections in the patterns, as outlined below.

Thermal Decomposition of α-$CaSO_4 \cdot 0.5D_2O$ (Experiment Number 4). Figure 6A displays a stack of SR-PXD patterns (numbers 1−35) for dry heating of α-$CaSO_4 \cdot 0.5D_2O$ corresponding to the temperature range of 25−217 °C. The pattern numbers 1−20 are from α-$CaSO_4 \cdot$

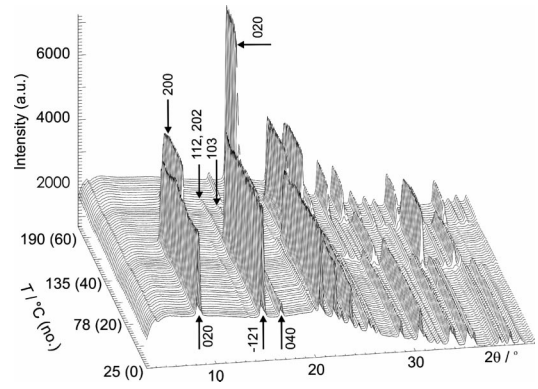

Figure 10. Stack of SR-PXD patterns showing the hydrothermal transformation of $CaSO_4 \cdot 2H_2O$ in a 1 M LiCl solution to α-$CaSO_4 \cdot 0.5H_2O$ at 123 °C and to insoluble anhydrite, AII-$CaSO_4$, at 190 °C ($\lambda = 1.1072$ Å). Miller indices indicated are the same as in Figure 9.

$0.5D_2O$; e.g., pattern number 15 (104 °C) corresponds to the unit cell parameters $a = 12.027(1)$, $b = 6.918(1)$, $c = 12.613(1)$ Å, $\beta = 90.29(1)°$, and the space group *I*121. Figure 7A displays the profile-matching Rietveld refinement of α-$CaSO_4 \cdot 0.5D_2O$ using pattern number 15.

A phase transition is observed at 138 °C (pattern number 21) as an increase in the background level and changes in the intensities of reflections from α-$CaSO_4 \cdot 0.5D_2O$. This observation is assigned to the formation of β-$CaSO_4 \cdot 0.5D_2O$, which exists to 186 °C (number 30). Figure 7B displays the profile-matching Rietveld refinement of β-$CaSO_4 \cdot 0.5D_2O$ using pattern number 25 at 160 °C, giving the unit cell parameters $a = 6.9457(4)$, $c = 12.5846(3)$ Å, and $V = 525.8$ Å^3, using the space group $P3_1$. The weak reflections of the monoclinic α-$CaSO_4 \cdot 0.5D_2O$, indicated with arrows in Figure 7A, are not observed in Figure 7B. The first strong reflection in Figure 7B has a larger intensity than the corresponding reflection in Figure 7A, and the background level in Figure 7B, at $2\theta = 11.0°$, is also higher than the background at the same position in Figure 7A. The *d* spacings of the SR-PXD pattern of number 25 are in good agreement with the ICDD card number 83-440 for β-$CaSO_4 \cdot 0.6D_2O$.

A second phase transition is observed at pattern number 29-30 (186 °C). The background level of the pattern is reduced considerably and so are the intensities of the strong reflections. Figure 6B displays a stack of powder patterns (numbers 35–85), corresponding to the temperature range from 215 to 490 °C. The patterns show reflections from soluble anhydrite, AIII-$CaSO_4$, but additional reflections with increasing intensities from insoluble anhydrite, AII-$CaSO_4$, are observed in the entire temperature range. Figure 7C displays a profile-matching Rietveld refinement of soluble anhydrite, AIII-$CaSO_4$, using pattern number 36 measured at 222 °C giving the unit cell parameters $a = 6.9594(4)$, $c = 6.2852(7)$ Å, and $V = 263.6$ Å^3, using the space group $P6_222$.

These two phases, soluble and insoluble anhydrite, therefore coexist, and the latter is formed in depletion of soluble

(46) Favre-Nicolin, V.; Cerny, R. *Mater. Sci. Forum* **2004**, *443–444*, 35.
(47) Rietveld, H. M. *J. Appl. Crystallogr.* **1969**, *2*, 65.
(48) Solberg, C.; Hansen, S. *Cem. Concr. Res.* **2001**, *31*, 641.
(49) Oetzel, M.; Heger, G.; Koslowski, T. *ZKG Int.* **2000**, *53*, 354.

Table 5. Summary of Decomposition Temperatures *T* (°C) Found in the Present Investigation[a]

experiment number−dry heating				
reactants	$CaSO_4 \cdot 2H_2O$	α-$CaSO_4 \cdot 0.5H_2O$	α-$CaSO_4 \cdot 0.5D_2O$	β-$CaSO_4 \cdot 0.5D_2O$
products	α-$CaSO_4 \cdot 0.5H_2O$	AIII-$CaSO_4$	β-$CaSO_4 \cdot 0.5D_2O$	AIII-$CaSO_4$
		T (°C)		
number 2	109−140	165−172		
number 4			138	186
experiment number−hydrothermal heating				
reactants	$CaSO_4 \cdot 2H_2O$	α-$CaSO_4 \cdot 0.5H_2O$	β-$CaSO_4 \cdot 0.5H_2O$ α-$CaSO_4 \cdot 0.5H_2O$	α-$CaSO_4 \cdot 0.5H_2O$
products	α-$CaSO_4 \cdot 0.5H_2O$	β-$CaSO_4 \cdot 0.5H_2O$	AIII-$CaSO_4$	AII-$CaSO_4$
		T (°C)		
number 3 (H_2O)	99	118	169	
number 5 (1 M LiCl)	118			190
number 6 (1 M HNO_3)	123			190

[a] Reactants are listed above decomposition products, and the reaction temperatures are found in the different experiments.

anhydrite. A quantitative phase analysis was made using a selection of powder diffraction patterns and full profile refinements and crystallographic data for the structures of soluble anhydrite, given in Table 4, and insoluble anhydrite.[21] The results of this investigation are displayed in Figure 8 showing the quantity of the two forms of anhydrite versus the temperature. It is notable that the two forms of anhydrite coexist and that the formation of insoluble anhydrite starts already at approximately 200 °C. Second, the two curves cross at ca. 50%, indicating that the transformation of AIII to AII anhydrite proceeds without the presence of intermediate phases.

The thermal decomposition of α-$CaSO_4 \cdot 0.5D_2O$ thus proceeds via the formation of β-$CaSO_4 \cdot 0.5D_2O$ to form AIII-$CaSO_4$, which gradually transforms to insoluble $CaSO_4$ in the temperature range of 200−490 °C. In previous studies, the existence of β-$CaSO_4 \cdot 0.5H_2O$ was not observed as an intermediate phase during thermal decomposition of gypsum to anhydrite; i.e., one phase transition was reported of gypsum to $CaSO_4 \cdot 0.5H_2O$ at 70 °C and one for $CaSO_4 \cdot 0.5H_2O$ to anhydrite at 280 °C.[52] Similarly, dry dehydration of $CaSO_4 \cdot 2H_2O$ studied by powder neutron diffraction revealed only one subhydrate, which coexisted with gypsum in the temperature interval from 57 to 101 °C and a mixture of the anhydrites AIII- and AII-$CaSO_4$ in the temperature interval from 252 to 269 °C.[53]

Hydrothermal Decomposition of Gypsum in Acidic and Ionic Solution (Experiment Numbers 5 and 6). The stability of gypsum in acidic solution is displayed in Figure 9 as a stack of powder diffraction patterns. A phase transition is observed at 118 °C, where $CaSO_4 \cdot 2H_2O$ is converted to α-$CaSO_4 \cdot 0.5H_2O$. Under these conditions, the α-subhydrate is stable to 190 °C, where it converts directly to insoluble anhydrite, AII-$CaSO_4$. According to previous investigations, hydrothermal treatment of $CaSO_4 \cdot 2H_2O$ with a HNO_3 solution or with water yields α-$CaSO_4 \cdot 0.5H_2O$.[22]

The stability of gypsum in a salt solution, i.e., 1 M LiCl, is displayed in Figure 10 as a stack of SR-PXD patterns. A phase transition is observed at 123 °C, where $CaSO_4 \cdot 2H_2O$ is converted to α-$CaSO_4 \cdot 0.5H_2O$. The next phase transition is observed at 190 °C, where α-$CaSO_4 \cdot 0.5H_2O$ also transforms directly to insoluble anhydrite, AII-$CaSO_4$, in analogy to the observations reported above. According to previous investigations, hydrothermal treatment of $CaSO_4 \cdot 2H_2O$ with a 1 M LiCl solution is expected to yield β-$CaSO_4 \cdot 0.5H_2O$,[54] but in the present study, α-$CaSO_4 \cdot 0.5H_2O$ was formed. However, treatment with more concentrate solutions of LiCl has been reported to yield α-$CaSO_4 \cdot 0.5H_2O$.[54]

The hydrothermal decomposition of $CaSO_4 \cdot 2H_2O$ in acidic or ionic solutions goes via the transformation of α-$CaSO_4 \cdot 0.5H_2O$ to insoluble anhydrite. For the two experiments performed, the results are partly in agreement with previous investigations.[22,54] It is notable that insoluble anhydrite is formed as a pure phase without any traces of soluble anhydrite. Soluble anhydrite is known to react readily with water to give gypsum $CaSO_4 \cdot 2H_2O$, and this is not the case for insoluble anhydrite. The water-free calcium sulfate found in nature as a mineral is insoluble anhydrite.[21]

4. Conclusion

Calcium sulfates, in particular gypsum and the subhydrates, are used in a number of large-scale industrial applications. Their structures and transformations remained not fully understood, which prompted the present study. The structures of β-$CaSO_4 \cdot 0.5H_2O$ and soluble $CaSO_4$ were reinvestigated, and revised structural models are presented.

The α-$CaSO_4 \cdot 0.5H_2O$ hydration experiment shows that the depletion of α-$CaSO_4 \cdot 0.5H_2O$ is correlated with the increase in quantity of $CaSO_4 \cdot 2H_2O$ as a typical dissolution diffusion, nucleation, and growth process.[55] The result shows that the previous interpretation of the powder neutron diffraction data is in error.[51] The decomposition temperatures found experimentally are listed in Table 5. The thermal decomposition of $CaSO_4 \cdot 2H_2O$ gives initially α-$CaSO_4 \cdot 0.5H_2O$, which converts to AIII-$CaSO_4$. The hydrothermal decomposition of $CaSO_4 \cdot 2H_2O$ revealed β-$CaSO_4 \cdot 0.5H_2O$ as an intermediate, which also converts to AIII-$CaSO_4$. In contrast to gypsum, the thermal decomposition of α-$CaSO_4 \cdot 0.5D_2O$ proceeds with β-$CaSO_4 \cdot 0.5D_2O$ as an intermediate phase prior to the formation of soluble anhydrite. It has previously been questioned whether β-$CaSO_4 \cdot 0.5H_2O$ exists as a pure phase, but the phase is obtained in the present paper and other indepen-

(50) Oetzel, M.; Scherberich, F.-D.; Heger, G. *Powder Diffr.* **2000**, *15*, 30.
(51) Christensen, A. N.; Lehmann, M. S.; Pannetier, J. *J. Appl. Crystallogr.* **1985**, *18*, 170–172.
(52) Cernik, R. J. *SRS Annu. Rep.* **2002–2003**, 1.
(53) Abriel, W.; Reisdorf, K.; Pannetier, J. *J. Solid State Chem.* **1990**, *85*, 23.

dent studies.[23] The formed water-free $CaSO_4$ is a mixture of soluble and insoluble anhydrite, where the quantity of the latter is increasing with an increasing temperature. Hydrothermal decomposition of $CaSO_4 \cdot 2H_2O$ in 1 M HNO_3 or 1 M LiCl solutions converted gypsum to α-$CaSO_4 \cdot 0.5H_2O$ and then directly to insoluble anhydrite, AII-$CaSO_4$. It is notable that soluble anhydrite, AIII-$CaSO_4$, was not formed in these two experiments.

Acknowledgment. T.R.J. gratefully acknowledges the Carlsberg Foundation for financial support. We also thank The Danish National Research Council under Dansync.

CM7027542

(54) Marinkovic, S.; Kostic-Pulek, A.; Djuricic, M. *J. Serb. Chem. Soc.* **2000**, *65*, 265.

(55) Goto, T.; Ridge, M. J. *Aust. J. Chem.* **1965**, *18*, 769–776.